Bioactive Materials 18 (2022) 42–55

Contents lists available at ScienceDirect

Bioactive Materials

journal homepage: www.keaipublishing.com/en/journals/bioactive-materials

Molecularly engineered tumor acidity-responsive plant toxin gelonin for safe and efficient cancer therapy

Guo-Bin Ding [a,**], Chenchen Zhu [a], Qian Wang [a], Huiyan Cao [a], Bin-Chun Li [a], Peng Yang [a], Roland H. Stauber [a,c], Guangjun Nie [b,*], Zhuoyu Li [a,***]

[a] Institute of Biotechnology, The Key Laboratory of Chemical Biology and Molecular Engineering of Ministry of Education, Shanxi University, Taiyuan, 030006, China
[b] CAS Key Laboratory for Biomedical Effects of Nanomaterials & Nanosafety, National Center for Nanoscience and Technology, Beijing, 100190, China
[c] Nanobiomedicine Department/ENT, University Medical Center Mainz, Mainz, 55131, Germany

ARTICLE INFO

Keywords:
Gelonin
Biosynthesis
pHLIP
Tumor-acidity responsive
Apoptosis
Cancer therapy

ABSTRACT

Due to the unsatisfactory therapeutic efficacy and inexorable side effects of small molecule antineoplastic agents, extensive efforts have been devoted to the development of more potent macromolecular agents with high specificity. Gelonin is a plant-derived protein toxin that exhibits robust antitumor effect via inactivating ribosomes and inhibiting protein synthesis. Nonetheless, its poor internalization ability to tumor cells has compromised the therapeutic promise of gelonin. In this study, a tumor acidity-responsive intracellular protein delivery system — functional gelonin (Trx-pHLIP-Gelonin, TpG) composed of a thioredoxin (Trx) tag, a pH low insertion peptide (pHLIP) and gelonin, was designed and obtained by genetic recombination technique for the first time. TpG could effectively enter into tumor cells under weakly acidic conditions and markedly suppress tumor cell proliferation via triggering cell apoptosis and inhibiting protein synthesis. Most importantly, treatment by intravenous injection into subcutaneous SKOV3 solid tumors in a mouse model showed that TpG was much more effective than gelonin in curtailing tumor growth rates with negligible toxicity. Collectively, our present work suggests that the tumor acidity-targeted delivery manner endowed by pHLIP offers a new avenue for efficient delivery of other bioactive substances to acidic diseased tissues.

1. Introduction

As the cornerstone treatment modality, chemotherapy is still an indispensable strategy for cancer therapy, but its clinical outcome is far from satisfactory [1,2]. Traditional chemotherapy primarily depends on small-molecule drugs [3], and is often accompanied with severe side effects due to the lack of selectivity towards cancerous tissues and the undesirable distribution in normal tissues [1,4,5]. Since recombinant human insulin was approved as the first therapeutic protein for clinical applications, the development of protein-based macromolecular cancer therapeutics has been an utmost focus of research [6,7]. Therapeutic proteins and peptides accounts for approximately 85% of the currently approved ~300 biopharmaceutical drugs. [7], and seven of the top ten best-selling drugs worldwide in 2018 belong to protein [8,9]. Albeit protein agents display prominent advantages over small-molecule drugs, such as unmatched potency, high specificity to their intracellular targets and low toxicity [4,10–13], their clinical translation has been undermined by several unfavorable intrinsic characteristics including large size, hydrophilicity, membrane impermeability and susceptibility to enzymatic degradation [10,11]. Thus, a variety of delivery approaches have been exploited for intracellular and cytosolic delivery of proteins [14–19].

Gelonin is a 30 kDa single chain glycoprotein originally derived from the seeds of *Gelonium multiflorum* [20]. As a type I ribosome inactivating protein (RIP) phytotoxin, it inhibits protein synthesis by cleaving the adenine 4324 of 28S ribosomal RNA, resulting in cell death [21]. Gelonin exhibits excellent performance in inhibiting protein translation, and it has been reported that 1–10 gelonin molecules can kill one tumor cell after cellular entry [22,23]. However, due to the lack of membrane binding domain, gelonin itself cannot enter cells, which severely limits

Peer review under responsibility of KeAi Communications Co., Ltd.
* Corresponding author.
** Corresponding author.
*** Corresponding author.
E-mail addresses: dinggb2012@sxu.edu.cn (G.-B. Ding), niegj@nanoctr.cn (G. Nie), lzy@sxu.edu.cn (Z. Li).

https://doi.org/10.1016/j.bioactmat.2022.02.001
Received 15 November 2021; Received in revised form 17 January 2022; Accepted 7 February 2022
Available online 11 February 2022

its clinical utility as a potent antitumor agent [24–26]. Hence, different technologies have been proposed during the last decade aiming at enhancement of the cellular internalization and tumor targeting ability of gelonin. Yang and Shin et al. integrated membrane-active peptides (e.g. TAT peptide, melittin and low molecular weight protamine) or tumor targeting molecules (such as F3 peptide, anti-insulin-like growth factor-1 receptor affibody and chlorotoxin) into gelonin by chemical conjugation or expressing a fusion protein to improve its cellular penetration and antitumor activity [27–35]. Moreover, extracellular vesicle membrane (EVM)-camouflaged metalorganic framework (MOF)

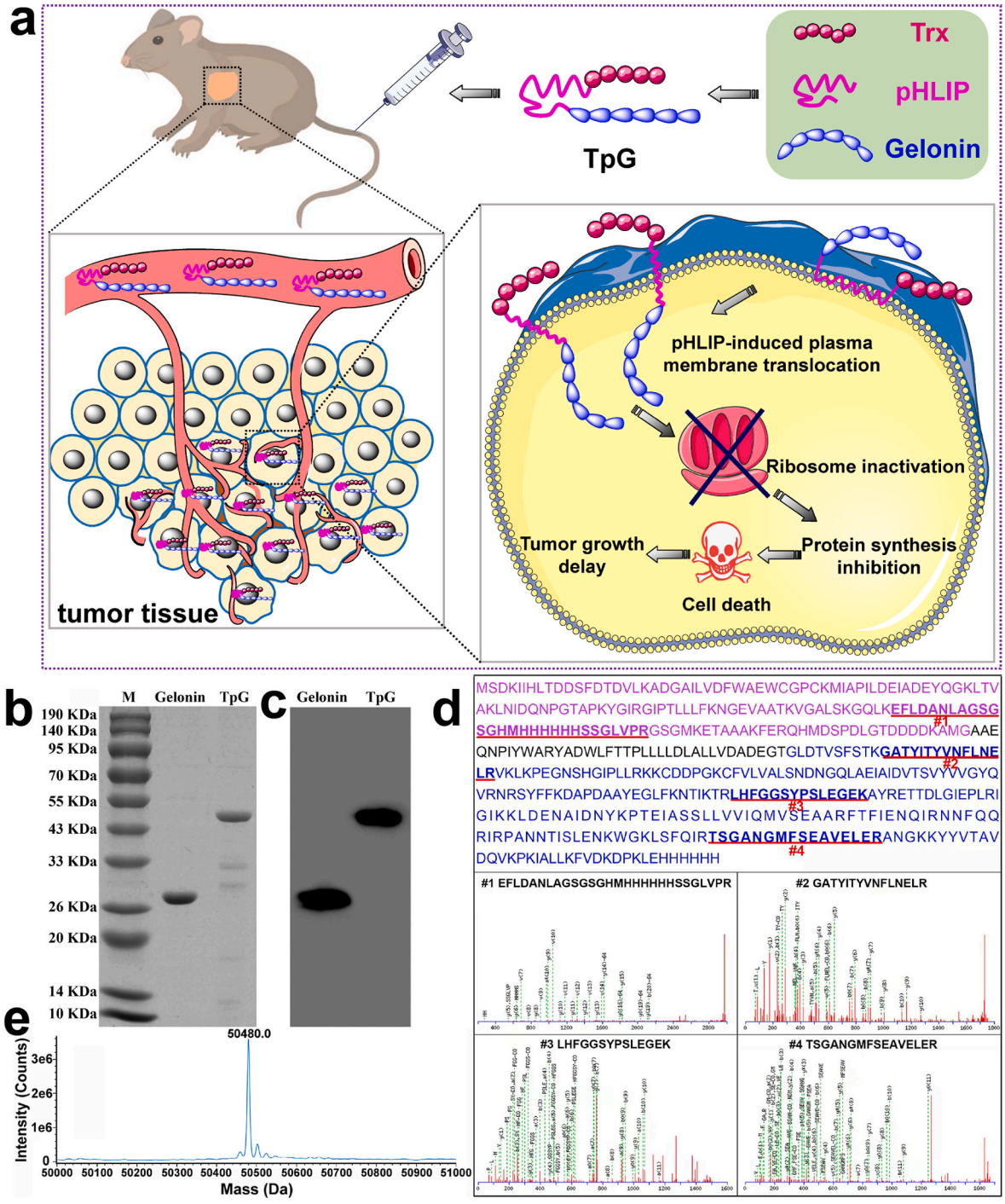

Fig. 1. Schematic illustration of the structure, mechanism of action and characterization of functional gelonin TpG. (a) TpG consists of three different fragments with distinct functions — a thioredoxin (Trx) tag improves solubility and enhances metabolic stability of the therapeutic protein, a pHLIP facilitates tumor acidity-responsive intracellular delivery of gelonin into tumor cells, and the toxin protein gelonin exerts antitumor activity. After injection into tumor-bearing mice, TpG could effectively accumulate in weakly acidic tumor tissues (pH 6.5), form an α-helix across the plasma membrane and specifically deliver gelonin locates at its C-terminus to cancer cells. TpG can irreversibly inactivate ribosomes, trigger a massive cell death via inhibiting protein synthesis and thereby hinder tumor growth. (b) SDS-PAGE of purified gelonin and TpG. Lane M is a protein molecular weight marker; lane Gelonin and TpG are purified gelonin and TpG, respectively. (c) Western blot analysis of purified gelonin and TpG by using anti-His antibody. (d) Mass spectrometry analysis of the TpG band cut from the SDS-PAGE gel, which shows the presence of four representative peptide fragments (#1–4) after proteolysis that match the theoretical amino acid sequence of TpG. Sequences of Trx, pHLIP and gelonin were shown in purple, black and blue respectively. (e) Deconvoluted mass spectra of TpG as determined by LC-MS.

nanoparticles were employed for efficient intracellular delivery of gelonin [36]. The aforementioned tumor-targeting approaches mainly depend on the passive targeting based on enhanced permeation and retention (EPR) effect or biomarker-targeting ligands-directed active targeting, which are also the commonly used targeting strategy for small molecules-encapsulated nanocarriers [37,38]. Nonetheless, these two targeting modalities face formidable challenges in recent years and their efficacy is compromised by the great pathophysiological heterogeneity of large tumors [39,40]. Therefore, it is imperative to develop a general and efficient tumor targeting strategy for gelonin delivery without relying on EPR effect or on endogenous biomarkers.

Extracellular acidosis (pHe <6.8) is a detrimental characteristic stemming from the aerobic glycolysis (Warburg effect) [41]. Tumor acidity is an important hallmark at almost every stage of tumor progression, and could be harnessed for tumor detection and targeted therapy [42]. Therefore, scientists have fabricated diverse pH-sensitive nanoscale drug delivery systems to achieve targeted drug delivery and improve tumor treatment efficiency [43,44]. However, most of these pH-responsive drug delivery systems require exquisite design, meanwhile researchers need to have a strong background in organic synthesis. pH low insertion peptide (pHLIP) is a 36-amino acids peptide originated from bacteriorhodopsin C helix, which could form a transmembrane α-helix and translocate cell-impermeable cargoes that are conjugated to its C terminus across a cell membrane under acidic conditions [45]. pHLIP-mediated targeting strategy based on tumor acidic microenvironment is significantly superior to traditional passive and active targeting in many respects [46]. Thus, pHLIP has been tremendously utilized for delivery of a wide range of theranostic molecules to achieve specific tumor imaging or enhanced therapeutic index [47–54].

To overcome the above-mentioned limitations of current gelonin delivery strategies and take advantage of the pH-responsive membrane permeation ability of pHLIP, herein we innovatively proposed an intracellular protein delivery system and biosynthesized a functional gelonin (denoted as Trx-pHLIP-Gelonin, TpG) by genetic engineering method. TpG is comprised of three different fragments with specific functions — a thioredoxin (Trx) tag, a pHLIP with a sequence of AAEQNPIYWARYADWLFTTPLLLLDLALLVDADEGT and the plant toxin gelonin (Fig. 1a). Trx is a highly hydrophilic and thermally stable protein with chaperone-like activity. It has been well documented that Trx is frequently employed as a fusion partner to improve the stability of recombinant protein and prevent inclusion body formation [55,56].

As depicted schematically in Fig. 1a, when intravenously injected into the tumor-bearing mice, TpG could effectively enter tumor cells under the guidance of pHLIP, initiating cell apoptosis via restraining protein synthesis and thereby impeding the tumor growth (Fig. 1a). The obtained TpG was systematically characterized, and its cellular uptake behavior and antiproliferative effect were tested in three different cancer cell lines. Moreover, the *in vivo* antitumor efficacy of TpG was demonstrated in an SKOV3 subcutaneous xenograft model by intravenous administration.

2. Materials and methods

2.1. Materials

Competent *Escherichia coli* BL21 (DE3) and protein marker (10–190 kDa) were obtained from Beijing TansGen Biotech (Beijing, China). Ni-nitrilotriacetic acid (NTA) resin and primary antibody against His-tag were provided by Suzhou Biodragon Immunotechnologies Co., Ltd (China) and Yeasen Biotechnology (Shanghai) Co., Ltd (China), respectively. Bicinchoninic acid (BCA) protein assay kit and carboxyfluorescein diacetate succinimidyl ester (CFDA-SE) cell proliferation assay kit were purchased from Beyotime Institute of Biotechnology (China). Fluorescein isothiocyanate (FITC) was obtained from Apeptide Co., Ltd. (Shanghai, China). Live/dead cell double staining kit, Annexin V/PI double staining apoptosis detection kit and caspase-3 activity assay kit were provided by BestBio (Shanghai, China). EdU assay kit was purchased from Sangon Biotech Co., Ltd. (Shanghai, China). Primary antibodies against PCNA, Ki-67, Bcl-2 and p53 were obtained from Beijing Bioss Biotechnology Co., Ltd (China).

2.2. Expression and characterization of Trx-pHLIP-Gelonin (TpG)

The *pHLIP-Gelonin* gene sequence was synthesized by Sangon Biotech Co., Ltd. (Shanghai, China). The expression vector pET32a-*pHLIP-Gelonin* was constructed by double digestion (*Xho* I and *Nco* I) of pUC57-*pHLIP-Gelonin* vector and pET32a vector, followed by ligation with T4 DNA ligase. pET32a-*pHLIP-Gelonin* was transformed into the competent *Escherichia coli* BL21 (DE3) and incubated at 37 °C. Isopropylthiogalactoside (IPTG) was added (final concentration: 0.5 mM) when optical density (OD) at 600 nm reached 0.6–0.8, and the culture was incubated overnight (at 16 °C, 180 rpm). Then cells were harvested by centrifugation, resuspended in 20 mM Tris (150 mM NaCl, pH 8.0), and lysed by sonication. Cell lysate was centrifuged at 12,000 rpm for 20 min and the supernatant was loaded onto Ni-NTA resin, washed with 20 mM Tris (80 mM imidazole, 150 mM NaCl, pH 8.0), and eluted with 20 mM Tris (200 mM imidazole, 150 mM NaCl, pH 8.0). The TpG protein solution was desalted and concentrated by ultrafiltration. The purified of TpG was monitored by sodium dodecyl sulphate polyacrylamide gel electrophoresis (SDS-PAGE) and western blot analysis. The purity of TpG was measured by densitometry analysis using ImageJ software and the production yield was determined using a BCA assay. After SDS-PAGE, the TpG band was cut out and digested into peptide fragments for mass spectrometry analysis. TpG was also subjected to liquid chromatography mass spectrometry (LC-MS) analysis for further characterization. Recombinant gelonin was obtained according to our previous report [26], and used as control in this study.

2.3. Thermal stability and serum stability of TpG

The inflection temperature (Ti) was monitored based on changes in intrinsic fluorescence at 330 nm and 350 nm using a Tycho NT.6 instrument (NanoTemper Technologies, Germany). Trx, gelonin and TpG with a concentration of 1 mg/mL were loaded in a glass capillary tube and heated from 35 °C to 95 °C at a rate of 30 °C/min. The ratio of fluorescence (350/330 nm) and the Ti value were calculated by Tycho NT.6. In addition, the thermal stability of TpG was assessed using a Chirascan circular dichroism (CD) spectrometer (Applied Photophysics, UK). The CD spectra of TpG (3.5 μM) in a range of 195–260 nm were collected at different temperatures (30, 35, 40, 45, 50, 55, 60, 65, 70, 75, 80, 85, 90, and 95 °C) at a heating rate of 2 °C/min, and the scanning speed is 1 nm/s. And the content of secondary structures was calculated via CDNN software.

For serum stability test, TpG (10 μM) was incubated at 37 °C in fresh medium containing 10% fetal bovine serum (FBS) at pH 7.4 or 6.5 for different time (0, 1, 2, 4, 6, 12, 24, and 48 h). Then the TpG was mixed with loading buffer and subjected to SDS-PAGE, the TpG band intensity was quantified using ImageJ software. And the TpG band intensity at 0 h was set as 100%.

2.4. Cellular uptake of TpG

FITC-labeled gelonin and TpG (FITC-Gelonin and FITC-TpG) were used to facilitate cellular internalization study. Three different cancer cell lines — human ovarian cancer cell line (SKOV3), human lung adenocarcinoma cell line (A549) and human colon cancer cell line (HCT-8) were seeded on glass coverslips in a 12-well plate and incubated for 24 h. Next, the medium was replaced with fresh medium (pH 7.4 or 6.5) containing FITC-Gelonin or FITC-TpG (with a concentration of 1 μM) and incubated for 12 h. The cells were washed three times with PBS, stained with DAPI for cell nuclei, and observed by Deltavision Elite Microscopy Imaging Systems (GE Healthcare).

For flow cytometric assay, SKOV3, A549 and HCT-8 cells were seeded into 12-well plates and incubated for 24 h, FITC-Gelonin or FITC-TpG (1 μM) in fresh medium (pH 7.4 or 6.5) was added and incubated for 12 h. The cells were harvested by trypsinization, washed twice with cold PBS, filtered through nylon mesh, and subjected to flow cytometric analysis using a Beckman Coulter CytoFLEX flow cytometer (Beckman Coulter, USA).

2.5. MTT cell viability assay

SKOV3, A549 and HCT-8 cells were seeded onto 96-well plates at a density of 3000 cells per well and incubated for 24 h. Cells were treated with gelonin or TpG of varying final concentrations (0.001, 0.01, 0.1, 1, and 10 μM) in fresh medium with a pH of 7.4 or 6.5 for 48 h. The cell viability was determined by MTT assay and the absorbance at 570 nm was measured using a microplate reader.

2.6. Crystal violet staining assay

SKOV3, A549 and HCT-8 cells were seeded onto 96-well plates at a density of 5000 cells per well and incubated for 24 h. The culture medium was replaced by fresh medium (pH 7.4 or 6.5), supplemented with gelonin or TpG of different concentrations (0.01, 0.1, and 1 μM), and incubated for 48 h. After addition of 0.5% crystal violet staining solution to each well and incubated for 20 min in a shaker, cells were rinsed thrice with PBS and observed under a light microscope. For cell viability quantitation, 200 μL of methanol was added to each well, incubated for 20 min at room temperature and the absorbance at 570 nm was determined to calculate cell viability.

2.7. Calcein AM/PI living/dead cell double staining

SKOV3, A549 and HCT-8 cells were seeded onto 96-well plates (5000 cells/well) and incubated for 24 h. Fresh medium (pH 7.4 or 6.5) including gelonin or TpG (1 μM) was added and incubated for 48 h. Then the cells were stained with Calcein-AM for 30 min and stained with PI for 5min, followed by washing twice with PBS. The images were acquired by fluorescent microscopy immediately. The Calcein-AM positive cells and PI-positive cells were counted in three separate fields, and the live cell ratio was calculated as the number of Calcein-AM positive cells divided by the number of total cells (Calcein-AM-positive cells plus PI-positive cells)

2.8. EdU staining

The EdU incorporation assay was performed according to the manufacturer's protocol. SKOV3 cells were seeded onto 24-well plates (2×10^5 cells/well) and incubated for 24 h. Cells were exposed to gelonin or TpG (1 μM) at pH 7.4 or 6.5 for 48 h, and incubated with EdU for 2 h. Then the cell nuclei were counterstained with Hoechst 33342, and cells were imaged with fluorescent microscopy immediately. EdU-positive cells and Hoechst 33342-positive cells were counted in three random separate fields. EdU positive rate was calculated as the number of EdU-positive cells divided by the number of total cells (Hoechst 33342-positive cells)

2.9. CFDA-SE cell proliferation assay

SKOV3 cells were trypsinized, harvested and stained with CFDA-SE according to the manufacturer's protocol. The CFDA-SE labeled cells were seeded into 12-well plates, incubated for 24 h, then gelonin or TpG (1 μM) in fresh medium (pH 7.4 or 6.5) was added and incubated for another 24 h. The cells were collected, washed twice with PBS, filtered, and the intensity of CFDA-SE in cells was analyzed using a Beckman Coulter CytoFLEX flow cytometer (Beckman Coulter, USA).

2.10. Determination of apoptosis by Annexin V/PI double staining

SKOV3 cells were seeded into 12-well plates, incubated for 24 h, and treated with gelonin or TpG (1 μM) in fresh medium (pH 7.4 or 6.5) for 48 h. Then the cells were harvested, washed twice with PBS, and stained with Annexin V-FITC and propidium iodide (PI) in the dark sequentially. Finally, the cells were resuspended in 400 μL binding buffer and the ratios of early (Annexin V-positive and PI-negative) and late (Annexin V-positive and PI-positive) apoptotic cells were recorded using a Beckman Coulter CytoFLEX flow cytometer (Beckman Coulter, USA). Meanwhile, the cell images were collected by fluorescent microscopy.

2.11. Measurement of caspase-3 activity

SKOV3 cells were seeded into 12-well plates and incubated for 24 h. The fresh media (pH 7.4 or 6.5) containing gelonin or TpG (1 μM) were added and incubated for 48 h. Subsequently, the cells were harvested, lysed, and the activity of caspase-3 was determined by using a caspase-3 activity kit in accordance with the manufacturer's protocol. Caspase-3 activity of the control group was set as 1, and the relative caspase-3 activity was presented as the ratio of enzyme activity in treated group to that of control group.

2.12. Intracellular protein inhibition assay

SKOV3 cells were seeded into 12-well plates and incubated overnight to allow the cells to attach to the bottom of cell plates. Then gelonin or TpG (1 μM) in fresh media (pH 7.4 or 6.5) was added and incubated for 48 h. The medium was aspirated, the cells were washed twice with cold PBS and lysed with 1% Triton X-100. The cell lysates were collected, and centrifuged at 12,000 rpm for 15 min. Finally, the total protein content in the supernatant was measured by BCA kit and the relative cellular protein levels were calculated by dividing the protein content in treated group by that of the untreated control group.

2.13. In vivo tumor suppression study

All of the animal experiments procedures were carried out with the approval of the Ethics Committee for the Management and Use of Laboratory Animals, China Institute for Radiation Protection (CIRP). Female BALB/c mice (four weeks old) were purchased from National Institutes for Food and Drug Control and housed in specific pathogen-free (SPF) barrier facilities. The SKOV3 subcutaneous ovarian cancer xenograft model was established by subcutaneously inoculation of 5×10^6 SKOV3 cells into the armpits of the right anterior limbs. Tumor size was measured with a digital caliper and calculated according to the equation: V (mm^3) = tumor length × (tumor width)^2/2. When the tumor volume reached about 200 mm^3 (set as day 0), the SKOV3 tumor-bearing mice were randomly divided into three groups (n = 7): control, gelonin, and TpG, and injected intravenously on days 0, 3, 6, and 9. The injection dose of gelonin and TpG was 0.35 μmol/kg. Saline (5 mL/kg) was injected in the control group. Tumor volume and body weight were monitored every 2 days for a period of 20 days. The relative tumor volume was defined as V/V_0 (V_0 is the tumor volume at day 0). The following formula was used to calculate the tumor growth inhibition ratio: (Vc−Vt)/Vc × 100%, where Vc and Vt are the average tumor volume of the control group and the treated group at day 20, respectively.

At day 20, all mice were euthanized, the blood of each mouse was collected, and the supernatant serum was obtained by centrifugation at 3000 rpm for 5 min. After blood sampling, tumors were dissected surgically and weighed, the major organs (heart, liver, spleen, lung, and kidney) were excised and fixed in 4% formaldehyde.

To evaluate histological changes in tumor, the paraffin-embedded tumors were sectioned into slices with a thickness of 5 μm and stained with hematoxylin and eosin (H&E). Furthermore, the expression of

PCNA, Ki-67, Bcl-2 and p53 in tumor sections dissected from the three groups of mice were analyzed by immunohistochemical staining.

2.14. In vivo biosafety evaluation

The paraffin-embedded normal tissues (heart, liver, spleen, lung, and kidney) were sectioned into 5 μm slices and stained with hematoxylin and eosin (H&E) to assess the histological changes. Besides, the blood biochemistry indicators including cardiac function parameters creatine kinase (CK), creatine kinase-MB (CK-MB), and lactate dehydrogenase (LDH) level; liver-associated alanine aminotransferase (ALT) and aspartate aminotransferase (AST); and renal function parameters blood urea nitrogen (BUN) and creatinine (Cr) levels were monitored by the corresponding commercial ELISA kits in accordance with the manufacture's protocols.

2.15. Statistical analysis

All the *in vitro* experiments were carried out three times independently. The *in vivo* antitumor experiments were conducted with 7 mice in each group. Data were expressed as the mean ± standard deviation (SD). Student's t-test was used to perform the statistical analysis for comparison between treatment and control groups, and difference was considered statistically significant when $P < 0.05$ (*) and highly significant when $P < 0.01$ (**).

3. Results and discussion

3.1. Biosynthesis and characterization of TpG

The expression vector pET32a-*pHLIP-Gelonin* was constructed and successfully transformed into the competent *E. coli* DH5α as confirmed by agarose gel electrophoresis (Fig. S1). Thioredoxin (Trx) tag is a hydrophilic and thermally stable protein and is widely used as fusion protein partner [51]. Thus, Trx was integrated at the N-terminus of pHLIP-Gelonin to endow it with excellent solubility and stability. Expression of TpG in *E. coli* BL21 (DE3) was induced by addition of 0.5 mM IPTG, and the soluble TpG was purified by Ni-NTA chromatography. The purified gelonin and TpG were identified by SDS-PAGE, and there is an intense band in both gelonin and TpG lanes at about 29 kDa and 51 kDa (Fig. 1b) respectively, suggesting the successful biosynthesis and purification of two recombinant proteins. The purity of gelonin and TpG was 95.00% and 91.24%, respectively, based on densitometry analysis of the SDS-PAGE gel. The final yield of the purified TpG was an average of 0.919 mg per liter of culture as determined by BCA protein assay. Western blot analysis using anti-His antibody further supported the SDS-PAGE results and verified the acquisition of His-tagged gelonin and TpG (Fig. 1c). The TpG band at about 51 kD was excised and digested into peptides for mass spectrometry analysis. Mass spectrometry analysis demonstrated the presence of 4 peptide fragments that matched partial sequences of TpG as shown in bold in Fig. 1d, and the sequence coverage rate of TpG was higher than 37%. LC-MS results indicated that there was only one major peak in HPLC chromatography of TpG with a retention time of 4.11 min (Fig. S2), indicating its high purity. Moreover, the molecular weight of TpG was 50.48 kDa as measured by LC-MS (Fig. 1e), which is consistent with the theoretical value (50.62 kDa) and SDS-PAGE results.

3.2. Thermal stability and serum stability of TpG

Thermal stability of proteins are critical for their biomedical applications [57]. To substantiate that the incorporation of Trx tag improves the thermal stability of gelonin, we performed label-free thermal shift analysis on a Tycho NT.6 instrument to evaluate the structural integrity (or folding) of the Trx, gelonin and TpG. As expected, Trx had a highest inflection temperature (Ti) of 82.4 °C, while gelonin showed the lowest Ti value of 71.5 °C (Fig. 2a). Interestingly, a Ti value of 76.5 °C was obtained for TpG (Fig. 2a), which is 5 °C higher than that of gelonin, suggesting TpG displayed better thermal stability as compared to gelonin. Next, circular dichroism (CD) spectra of TpG were collected at different temperatures to further assess its thermal stability. As shown in Fig. 2b, there is no appreciable change in the CD spectra in the range of 30–70 °C, whereas a marked variation in the CD spectra was observed when the temperature reaches above 75 °C, indicating that TpG had a good thermal stability and could maintain its secondary structure below 75 °C, which is also confirmed by the variations in the content of secondary structures (Table S1).

Serum half-life of therapeutic proteins is a key parameter affecting their effective delivery to specific cells or tissues [58]. An *in vitro* experiment was performed to gauge the serum stability of TpG in neutral or acidic (pH 7.4 or 6.5) 10% serum-containing medium. We could observe the bands of TpG at different time points even at 48 h and at both pH conditions with a small decrease in intensity (Fig. 2c and e), thus TpG remained stable after incubation with neutral or acidic cell medium for 48 h. Quantitative analysis of protein bands by Image J software showed that no significant degradation of TpG occurred after incubation in neutral and acidic medium for 48 h, and the protein band intensity was still higher than 75% (Fig. 2d and f). These results revealed that TpG exhibited excellent serum stability and might have a relative long serum half-life.

3.3. Cellular uptake profile of TpG

Penetration of proteins into the cytosol of mammalian cells or target tumor cells is a prerequisite for their therapeutic effects and remains a critical issue [59]. To enable visualization and quantitative analysis of the cellular internalization of TpG and gelonin in three different cancer cell lines — SKOV3, A549 and HCT-8, they were labeled with fluorescein isothiocyanate (FITC) (Fig. S3).

As shown in Fig. 3a, c and e, gelonin showed poor cellular uptake in three cells at both neutral and acidic conditions, and the FITC fluorescence intensity was pretty low. Under neutral conditions, the FITC intensity in TpG-treatment group was slightly higher than that of gelonin-treatment group. Intriguingly, the FITC intensity in TpG-treatment group was strikingly enhanced at pH 6.5. The quantitative analysis results (Fig. 3b, d and f) showed that the mean fluorescence intensity (MFI) of TpG treatment group under weakly acidic condition (pH 6.5) was significantly enhanced as compared to other groups. Consistent findings were obtained by determining the internalization of gelonin and TpG by DeltaVision Elite high-resolution imaging system, only some weak green spots were observed in gelonin-treated groups and TpG-treated group at pH 7.4, while a strong green fluorescence was clearly observed in TpG-treated group at pH 6.5 (Fig. S4). These results suggested that TpG did efficiently penetrate into different tumor cells under acidic conditions.

3.4. In vitro antitumor activity of TpG

Since TpG can effectively deliver gelonin into tumor cells under weakly acidic conditions, we next systematically investigated its *in vitro* antitumor activity. Firstly, three different tumor cells (SKOV3, A549 and HCT-8) were exposed to gelonin or TpG at five concentrations (0.001, 0.01, 0.1, 1, 10 μM) under neutral and acidic conditions for 48 h, and the cell viability was analyzed by MTT assay. It can be seen from Fig. 4 that gelonin and TpG displayed a dose-dependent inhibitory effect on the three tested cells, and no pH dependence was observed for the antitumor activity of gelonin. Unlike gelonin, TpG exhibited a pH-dependent cytotoxicity to three cells, and it outperformed gelonin at all tested concentrations under acidic conditions. The cell viabilities of SKOV3, A549 and HCT-8 cells treated with 10 μM TpG under weakly acidic conditions were 18.96 ± 2.35%, 35.27 ± 0.24% and 35.86 ± 2.97%, respectively. The IC_{50} values for gelonin and TpG were calculated from the MTT cytotoxicity data and are delineated in Table 1. TpG had lower

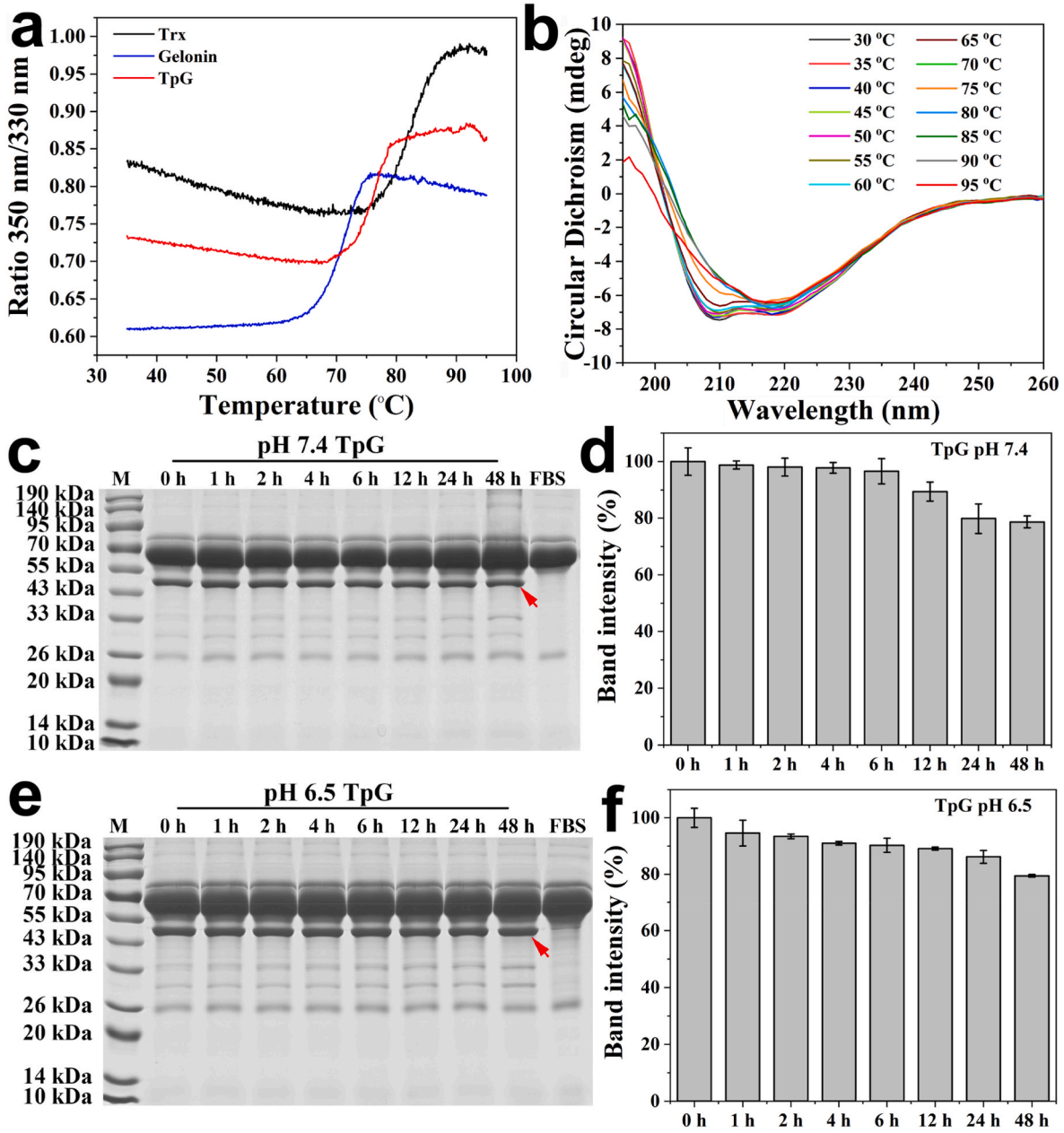

Fig. 2. Thermal stability and serum stability analysis of TpG. (a) Thermal expansion curves of Trx, gelonin and TpG plotted by the fluorescence ratio of 350 nm/330 nm. 1 mg/mL Trx, Gelonin or TpG was heated from 35 °C to 95 °C by Tycho NT.6 (NanoTemper Technologies), and the intrinsic fluorescence intensity of each protein at 330 nm and 350 nm was recorded. (b) CD spectra of TpG (3.5 μM) at different temperatures (30–95 °C). (c, e) SDS-PAGE of 10 μM TpG after incubation with 10% FBS-containing medium (pH 7.4 or 6.5) at 37 °C for different time. Lane M is a protein marker of 10–190 kDa, and FBS is the 10% FBS-containing medium. The red arrow indicates the band of TpG. Figures d and f show the quantitative analysis of TpG band in c and e using Image J software.

IC_{50} values than gelonin under both neutral and acidic conditions for the three tumor cells, and the lowest IC_{50} value was noted for TpG at pH 6.5 in SKOV3 cells (3.59 μM).

Crystal violet staining was also carried out to examine the inhibitory effect of TpG on the growth of the three tumor cells. Compared with control group, TpG decreased the number of viable cells in a dose- and pH-dependent fashion, while gelonin showed a concentration-dependent inhibition on cell growth but independent of pH (Figs. S5a, c, and e). Of note, quantitative analysis results suggested that the TpG treatment group under acidic conditions presented the strongest growth inhibitory activity at three drug concentrations and in all tested cell lines (Figs. S5b, d, and f). The percentages of viable SKOV3, A549 and HCT-8 cells were 34.59 ± 2.42%, 60.38 ± 2.91% and 69.36 ± 3.55%, respectively after treatment with 1 μM TpG at pH 6.5 for 48 h (Figs. S5b, d, and f). Moreover, the cytotoxic effect of TpG was further determined by live/dead staining assay, in which the calcein-AM/PI co-staining can distinguish the live/dead cells by green/red fluorescence. An intense green fluorescence was observed in gelonin-treated groups (both pHs), as well as in TpG-treated group under neutral conditions (Figs. S6a, c, and e), which is indicative of viable cells. By contrast, the emergence of strong red fluorescence in TpG-treated group under acidic conditions especially in SKOV3 cells (Figs. S6a, c, and e), illustrated that the cell death was clearly apparent. These observations were also supported by quantitative analysis of the live cell ratios (Figs. S6b, d, and f). We found that SKOV3 cells were the most sensitive to TpG among the three tested cells, thus this cell line was employed in the following experiments. The mechanism of action of gelonin is inhibiting the ribosome biogenesis. It has been reported that the ribosome biogenesis rate in different cancer

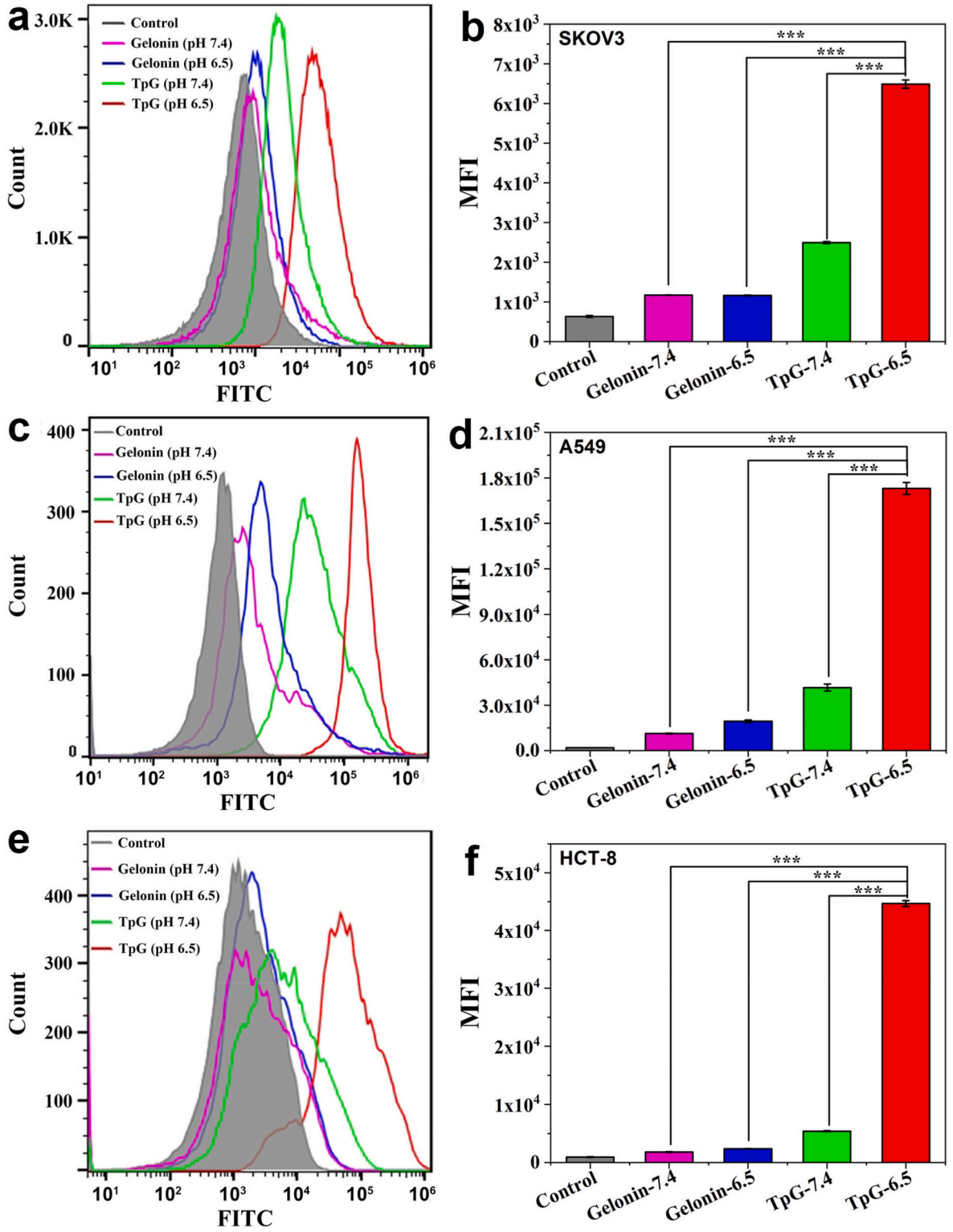

Fig. 3. Flow cytometry analysis of the cellular uptake of TpG in three tumor cells. SKOV3 (a, b), A549 (c, d) and HCT-8 cells (e, f) were incubated with 1 μM FITC-Gelonin and FITC-TpG at pH 7.4 or pH 6.5 for 12 h, and analyzed by flow cytometry. Figures b, d, and f show the mean fluorescence intensity (MFI) of different treatment groups in three tumor cells. The data are shown as the mean ± SD (n = 3). ***$P < 0.001$ as compared to TpG treated group at pH 6.5.

cells varies greatly, which account for their different sensitivity to antitumor agents [60]. And rRNA synthesis inhibitors exert strong antitumor activity only in the cells with high rates of ribosome biogenesis [60]. Therefore, the highest sensitivity of SKOV3 cell line to TpG may be attributed to its highest ribosome biogenesis rate among the three tested tumor cells. Furthermore, according to some previous reports, SKOV3 cell was indeed among the most sensitive cancer cell lines to gelonin treatment [61,62], while A549 cell was relatively insensitive to gelonin [63].

Afterwards, we continued to evaluate the antiproliferative effect of TpG on SKOV3 cells by EdU staining and CFDA-SE staining assay, the results were presented in Fig. 5. It can be seen from Fig. 5a that the red

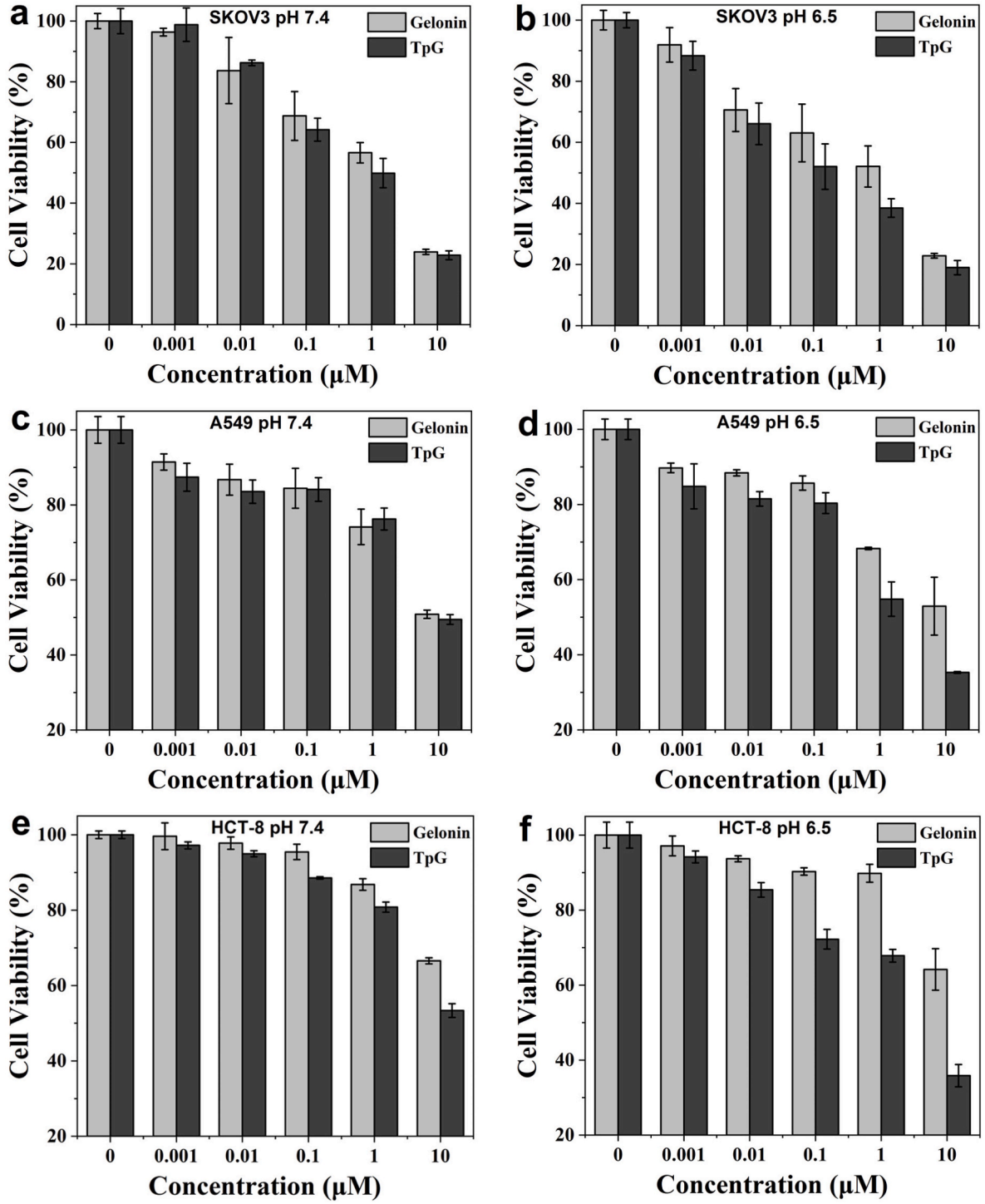

Fig. 4. Cell viability determination by MTT assay. Different concentrations (0, 0.001, 0.01, 0.1, 1, 1, 10 μM) of gelonin and TpG were incubated with SKOV3 cells (a, b), A549 cells (c, d) and HCT-8 cells (e, f) in neutral (pH 7.4) and acidic (pH 6.5) conditions for 48 h, and the relative cell viability of was measured by MTT assay.

Table 1
IC_{50} values of gelonin and TpG against SKOV3, A549, and HCT-8 cells.

Cell lines	IC_{50} (μM)			
	Gelonin		TpG	
	pH 7.4	pH 6.5	pH 7.4	pH 6.5
SKOV3	5.47	4.78	5.18	3.59
A549	9.89	10.22	9.68	6.70
HCT-8	12.82	12.79	10.36	7.20

fluorescence signal in SKOV3 cells decreased in varying degrees after treatment with gelonin and TpG, and the TpG-treated group under acidic conditions exhibited the weakest red fluorescence. Quantitative analysis showed that EdU-positive rates of gelonin-treated group at pH 7.4 and 6.5 were 32.26 ± 4.01% and 34.76 ± 1.03% respectively, while those of TpG-treated group were 31.32 ± 1.75% and 14.46 ± 1.98% respectively (Fig. 5b). As shown in Fig. 5c, the proportion of CFDA-SE positive cells treated with gelonin and TpG was significantly increased compared to the control group. Moreover, the anti-division activity was highly enhanced after 24 h treatment with TpG at pH 6.5, and the CFDA-

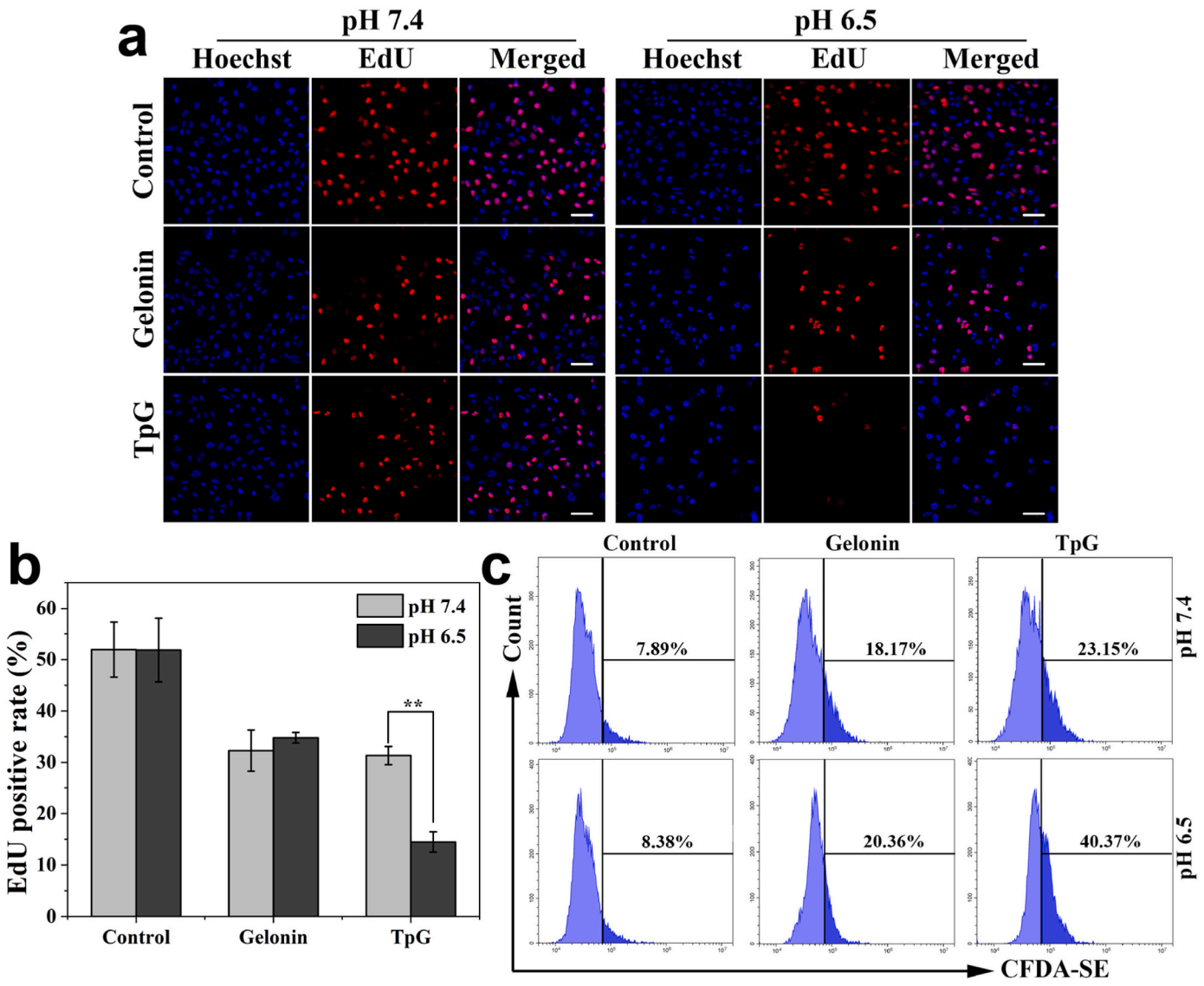

Fig. 5. Cell proliferation assay by EdU staining and CFDA-SE staining assay. (a) SKOV3 cells were exposed to 1 μM gelonin and TpG at pH 7.4 or pH 6.5 for 48 h, treated with EdU cell proliferation detection kit, and observed by high-resolution live-cell imaging system (scale bar: 50 μm). (b) quantitative analysis of the EdU-positive cell rates of different treated groups in figure a. **represents $P < 0.01$. (c) SKOV3 cells were labeled with CFDA-SE, and exposed to 1 μM gelonin and TpG at pH 7.4 or 6.5 for 24 h, the cell proliferation ability was analyzed by flow cytometry.

SE positive cells accounted for 40.37% (Fig. 5c). The above results revealed that TpG exerted pronounced inhibitory effect on the proliferation of SKOV3 cells under weakly acidic conditions (pH 6.5).

3.5. TpG triggers apoptosis and inhibits intracellular protein synthesis

To unravel the underlying mechanism of the antitumor activity, SKOV3 cells were exposed to 1 μM gelonin or TpG at pH 7.4 or pH 6.5 for 48 h, cell apoptosis was determined by Annexin V-FITC/PI double staining and caspase-3 activity assay kits, and the intracellular protein level was quantified using a BCA protein assay. As shown in Fig. 6a, the apoptotic cell rates of gelonin group (pH 7.4: 15.20%; pH 6.5: 17.33%) was comparable to TpG-treated group under neutral conditions (16.56%). Notably, TpG induced a much higher cell apoptosis rate (40.62%) at pH 6.5 than other groups. Both green fluorescence (Annexin FITC-positive) and red fluorescence (PI-positive) were significantly enhanced in TpG-treated cells at pH 6.5 as compared to other groups (Fig. 6b), which were in line with the flow cytometry results (Fig. 6a), indicating TpG noticeably boosted the cell apoptosis under weakly acidic conditions. The increase in cell apoptosis was associated with an elevated level of caspase-3 activity (1.06–2.00 folds of control) after exposure to gelonin or TpG (Fig. 6c), suggesting that they induced the activation of caspase-3. And the caspase-3 activity in cells incubated with TpG at pH 6.5 (2.00 folds of control) was much higher than other three groups (Fig. 6c), which were corresponding with the apoptotic cell rates obtained from flow cytometry analysis (Fig. 6a). Besides, to explore whether TpG retains the N-glycosidase activity of gelonin, the intracellular protein level was examined. After incubation with gelonin at pH 7.4 and 6.5, the relative protein levels were 81.05 ± 1.11% and 78.35 ± 0.98% respectively; similarly, the intracellular protein level of TpG treatment group at pH 7.4 was 78.27 ± 2.81% (Fig. 6d). Interestingly, TpG displayed significantly greater inhibition of protein translation at pH 6.5 with a relative protein level of 57.56 ± 2.57% (Fig. 6d). These results demonstrated that TpG exerted potent antitumor efficacy under weakly acidic conditions via inducing cell apoptosis and inhibiting protein translation.

3.6. TpG delayed tumor growth in vivo

With the validation of the augmented effectiveness of TpG in

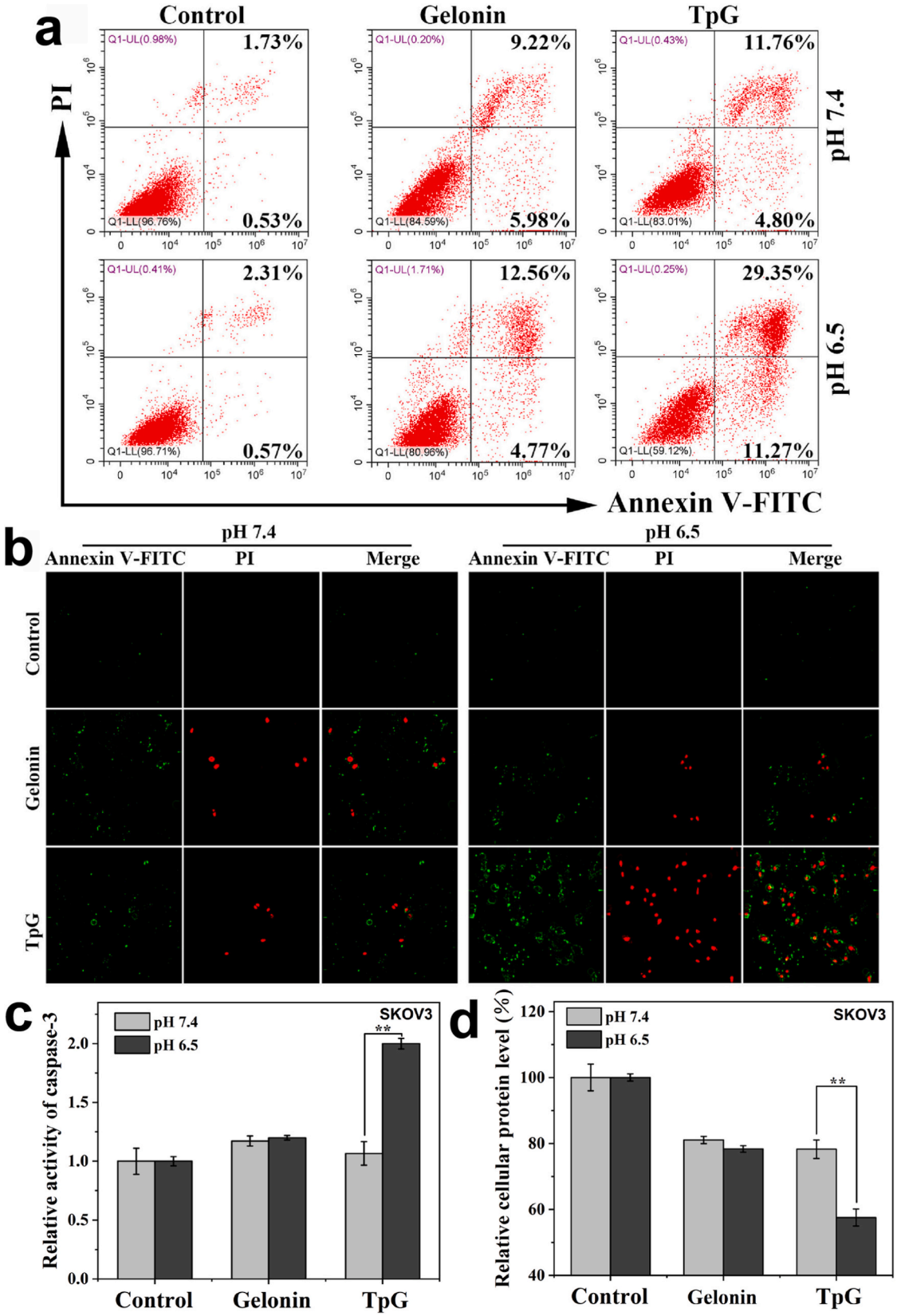

Fig. 6. TpG initiates apoptosis and suppresses intracellular protein synthesis. SKOV3 cells were treated with 1 μM Gelonin or TpG at pH 7.4 or pH 6.5 for 48 h. (a, b) Analysis of cell apoptosis by Annexin V-FITC/PI double staining. (a) Quantification of the cell apoptosis level by flow cytometry. (b) Images of SKOV3 cells observed by high-resolution live-cell imaging system (scale bar: 50 μm). (c) The relative activity of Caspase-3. (d) The relative intracellular protein level as determined by BCA protein assay kit. **represents $P < 0.01$.

inhibiting tumor cell proliferation *in vitro*, we next investigated the *in vivo* anticancer activity of TpG in human ovarian xenografts-bearing nude mice model, which were established by subcutaneously inoculation SKOV3 cells into the BALB/c mice. When the tumors reached about 200 mm^3, mice were intravenously administered with saline, gelonin or TpG every three days for a total of four times. Tumors in the saline control mice grew uncontrollably, and the relative tumor volume is 8.32 ± 0.50 (Fig. 7a). By comparison, treatment with gelonin or TpG could significantly inhibit tumor growth as compared with saline group with relative tumor volumes of 5.49 ± 0.57 and 2.57 ± 0.25, respectively. Inspiringly, the mice treated with TpG exhibited notably enhanced suppression of tumor growth, the relative tumor volume of gelonin-treated group was 2.14-fold of that in TpG-treated group. The tumor growth inhibitory ratios of gelonin and TpG were 33.91 ± 6.81% and 65.64 ± 3.31%, respectively (Fig. 7b). Eleven days after the last treatment (day 20), tumors in all groups were excised and weighed, both gelonin and TpG significantly reduced the tumor weights with relative tumor weights of 0.70 ± 0.08 and 0.31 ± 0.08, respectively (Fig. 7c). Obviously, the smallest relative tumor volume, highest inhibitory ratio and lowest weight of the tumors were observed in TpG-treated mice.

Histopathological and immunohistochemical analyses of tumor tissues after different treatments were performed to explore the potential mechanism underlying the *in vivo* antitumor activity of TpG. Hematoxylin and eosin (H&E) staining results indicated that tumor cells in saline group were intact and tightly aligned, and there is no indication of necrosis (Fig. 7d), suggesting the active cell proliferation. In stark contrast, different levels of necrosis occurred in tumor tissues of gelonin and TpG-treated group, and some typical signs of necrosis were observed, including decolorization of the nucleus, nuclear pyknosis and fragmentation of the tumor tissue (Fig. 7d), signifying a noticeable remission of tumor cells. Furthermore, tumor sections of different groups were subjected to immunohistochemical assay to analyze the expression of two proliferation-related proteins (PCNA and Ki-67) and two apoptosis-related proteins (Bcl-2 and p53). Compared with the saline group, the expression of PCNA, Ki-67 and anti-apoptosis protein Bcl-2 were significantly down-regulated, while the pro-apoptosis protein p53 were effectively upregulated in gelonin and TpG-treated groups (Fig. 7d). Interestingly, treatment with TpG produced much stronger effect than gelonin on inhibiting the expression of PCNA, Ki-67 and Bcl-2 and activating p53 (Fig. 7d). These results clearly demonstrated that gelonin

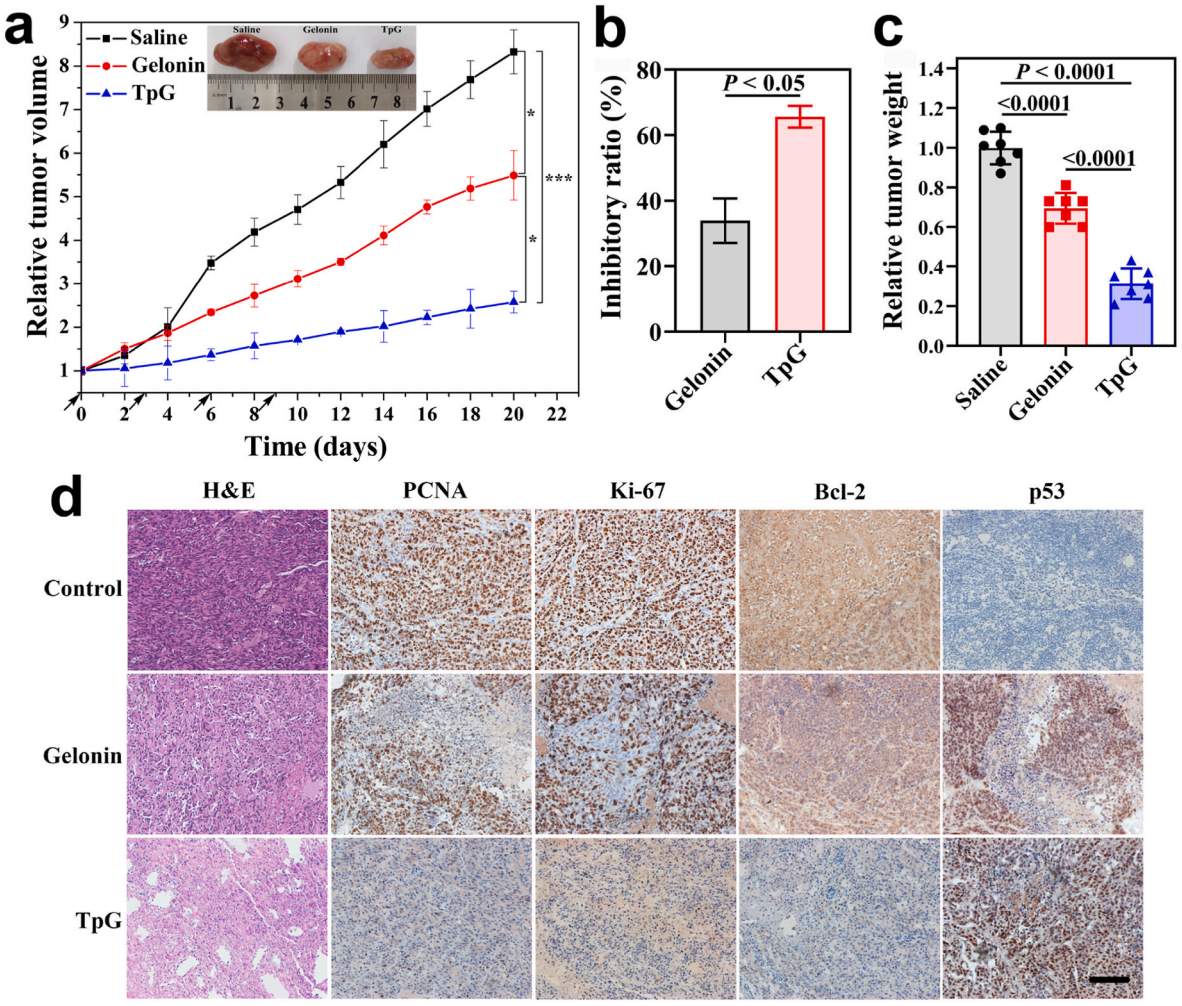

Fig. 7. TpG effectively suppresses tumor growth by inhibiting tumor cell proliferation and inducing tumor cell apoptosis. (a) Changes in relative tumor volume after treatment with saline, gelonin or TpG for a period of 20 days, the arrows indicated the administration time; the inset shows the representative photographs of tumor tissue of different groups at day 20. *represents $P < 0.05$ and ***represents $P < 0.001$. (b) Tumor growth inhibition ratio of gelonin and TpG. (c) Relative tumor weight of different treatment groups. The relative tumor weight was defined as the ratio of average tumor weight of gelonin or TpG-treated group to the average tumor weight of saline-treated group at day 20. (d) Representative images of tumor sections from different groups (saline, gelonin and TpG) after hematoxylin and eosin (H&E) and immunohistochemical staining for detection of PCNA, Ki-67, Bcl-2 and p53. The scale bar is 100 μm. Mice bearing SKOV-3 human ovarian xenografts (about 200 mm^3) were injected intravenously with different reagents (saline: 5 mL/kg; gelonin or TpG: 0.35 μmol/kg) every three day for a total of 4 injections (at day 0, 3, 6 and 9), tumor volume was monitored every 2 days for a period of 20 days.

and TpG robustly delayed tumor growth through inhibiting tumor cell proliferation and concomitantly stimulating tumor cell apoptosis. The good metabolic stability conferred by the thioredoxin (Trx) tag and pHLIP-mediated effective cellular internalization behavior of TpG accounted for its superior antitumor activity over gelonin.

3.7. *In vivo* biosafety evaluation of TpG

Considering that TpG elicited excellent efficacy in deferring tumor growth, we proceeded to evaluate its potential toxicity by monitoring the body weight changes of mice during the treatment period, H&E staining of normal tissues and determination of some serum biochemical parameters at day 20. The relative body weight of nude mice in each group fluctuated in a range of 0.97–1.12, and the relative body weight of gelonin and TpG treatment groups was slightly lower than that of the control group (Fig. S7).

H&E staining results showed that there were no incidences of main normal organ abnormalities in TpG-treated group as compared with the saline group, and hardly any pathological change in the cell morphology of normal tissues (heart, liver, spleen, lung, kidney) could be observed after TpG treatment (Fig. 8a). However, there were degenerative changes in myocardium in gelonin treatment group, such as myocyte vacuolization, interruption in continuity of myocardial fiber, nuclei loss in some muscle fibers (Fig. 8a). Similarly, a certain degree of pathological features of liver injury appeared in gelonin-treated group, including vacuolization of hepatocytes and nuclear contraction

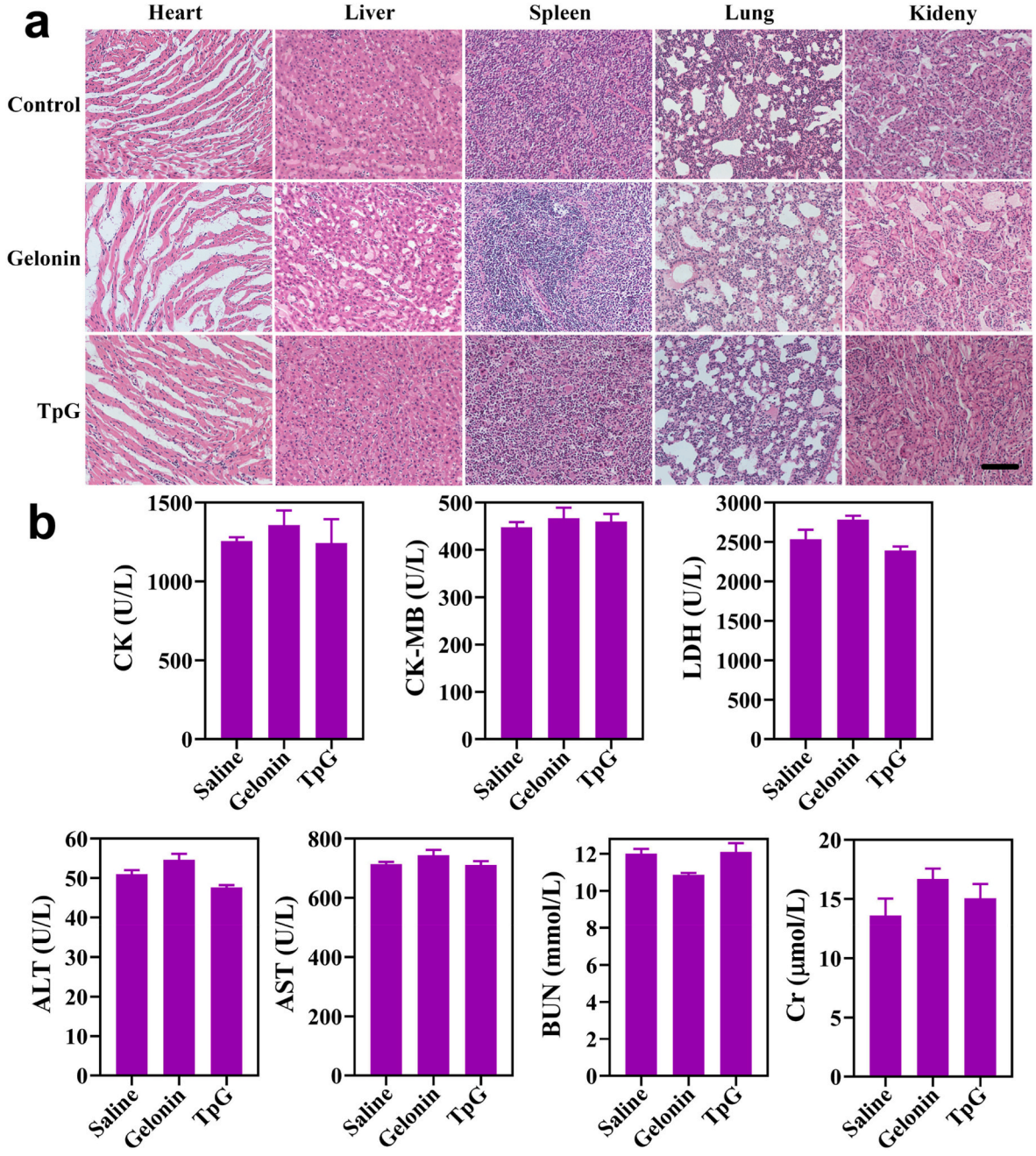

Fig. 8. *In vivo* biosafety assessment of TpG. (a) H&E staining analysis of the heart, liver, spleen, lung and kidney of SKOV3 tumor-bearing nude mice following different treatment groups via intravenous injection. The scale bar is 100 μm. (b) Determination of some serum biochemical indices after intravenous administration of saline, gelonin, and TpG: myocardial enzyme spectrum (creatine kinase, CK; creatine kinase isoenzyme, CK-MB; lactate dehydrogenase, LDH); liver function (alanine aminotransferase, ALT; aspartate aminotransferase, AST); renal function (blood urine nitrogen, BUN; creatinine, Cr).

(Fig. 8a). In addition, some changes in histopathological features of kidney (e.g. glomerular atrophy and nuclear aggregation) were detected after gelonin treatment (Fig. 8a). Analysis of serum biochemical indexes showed that all parameters in TpG group were close to those in control group; in contrast, CK, CK-MB, LDH, ALT, AST and Cr slightly increased in gelonin-treated group (Fig. 8b), which was consistent with the H&E staining results. The admirable biocompatibility of TpG may be attributable to its tumor acidity-targeting ability. These results revealed that TpG possessed favorable *in vivo* biosafety profile and held tremendous potential for the treatment of a wide variety of solid tumors.

4. Conclusion

We have molecularly engineered an effective gelonin delivery platform (Trx-pHLIP-Gelonin, TpG) by combining the advantages of Trx (metabolic stability and solubility improvement), pHLIP (pH responsiveness and high transmembrane capability) and gelonin (excellent antitumor efficacy). This platform is simple and cost-effective, and allows for reproducible expression of TpG with high purity (91.24%) and stable yield (0.94 mg/L). Furthermore, our delivery platform enabled an efficient intracellular translocation of gelonin in a pH-dependent manner. Notably, TpG manifested better cytotoxic activity against three different tumor cells (SKOV3, A549 and HCT-8) at pH 6.5 when compared to gelonin. Antitumor mechanistic studies revealed that TpG considerably caused cell apoptosis and suppressed protein synthesis, and eventually contributing to its antitumor property. Intriguingly, intravenous injection of TpG can effectively delay the tumor growth with minimal adverse effects in a subcutaneous tumor model of SKOV3 cells. Taken together, this functional gelonin fusion protein TpG holds great promise to be exploited as a safe and potent therapeutic agent for treating various solid tumors, and this delivery platform can be easily modulated by replacing gelonin with another bioactive protein, which allows broad utility of the delivery system.

CRediT authorship contribution statement

Guo-Bin Ding: Conceptualization, Methodology, Formal analysis, Data curation, Writing – original draft, Writing – review & editing, Funding acquisition, Supervision. **Chenchen Zhu:** Methodology, Investigation, Formal analysis, Data curation. **Qian Wang:** Methodology, Investigation, Formal analysis. **Huiyan Cao:** Methodology, Investigation, Formal analysis. **Bin-Chun Li:** Methodology, Formal analysis. **Peng Yang:** Methodology, Software. **Roland H. Stauber:** Funding acquisition, Writing – review & editing. **Guangjun Nie:** Conceptualization, Writing – review & editing, Supervision. **Zhuoyu Li:** Funding acquisition, Writing – review & editing, Supervision.

Declaration of competing interest

The authors declare that they have no known competing financial interests or personal relationships that could have appeared to influence the work reported in this paper.

Acknowledgements

This study was financially supported by National Natural Science Foundation of China (No. 31500771, 31770382), Research Project Supported by Shanxi Scholarship Council of China (No. 2021-016), Natural Science Foundation of Shanxi Province (No. 201901D111007, 201901D111013), foreign experts project of Shanxi Provincial “100 Talents Plan” (Prof. Roland H Stauber) and graduate education innovation project of Shanxi Province (2021Y120). We are grateful to Prof. Changxin Wu from Institutes of Biomedical Sciences of Shanxi University for sharing the multifunctional instrument platform. We acknowledge Ms. Xiedong Wang from Institutes of Biomedical Sciences of Shanxi University for her helpful discussion in flow cytometry analysis.

Appendix A. Supplementary data

Supplementary data to this article can be found online at https://doi.org/10.1016/j.bioactmat.2022.02.001.

References

[1] W. Shen, Y. Zhang, P. Wan, L. An, P. Zhang, C. Xiao, X. Chen, Antineoplastic drug-free anticancer strategy enabled by host-defense-peptides-mimicking synthetic polypeptides, Adv. Mater. 32 (2020) 2001108.
[2] G.B. Ding, H.Y. Liu, Y.Y. Lv, X.F. Liu, Y. Guo, C.K. Sun, L. Xu, Enhanced in vitro antitumor efficacy and strong anti-cell-migration activity of a hydroxycamptothecin-encapsulated magnetic nanovehicle, Chem. Eur J. 18 (2012) 14037–14046.
[3] G. Li, B. Sun, Y. Li, C. Luo, Z. He, J. Sun, Small-molecule prodrug nanoassemblies: an emerging nanoplatform for anticancer drug delivery, Small 17 (2021) 2101460.
[4] C. He, Z. Tang, H. Tian, X. Chen, Co-delivery of chemotherapeutics and proteins for synergistic therapy, Adv. Drug Deliv. Rev. 98 (2016) 64–76.
[5] G.B. Ding, J. Sun, P. Yang, B. Li, Y. Gao, Z. Li, A novel doxorubicin prodrug with GRP78 recognition and nucleus-targeting ability for safe and effective cancer therapy, Mol. Pharm. 15 (2018) 238–246.
[6] R. Zaman, R.A. Islam, N. Ibnat, I. Othman, A. Zaini, C.Y. Lee, E.H. Chowdhury, Current strategies in extending half-lives of therapeutic proteins, J. Contr. Release 301 (2019) 176–189.
[7] G.L. Beilhartz, S.N. Sugiman-Marangos, R.A. Melnyk, Repurposing bacterial toxins for intracellular delivery of therapeutic proteins, Biochem. Pharmacol. 142 (2017) 13–20.
[8] J. Lv, Q. Fan, H. Wang, Y. Cheng, Polymers for cytosolic protein delivery, Biomaterials 218 (2019) 119358.
[9] L. Urquhart, Top drugs and companies by sales in 2018, Nat. Rev. Drug Discov. 18 (2019) 245.
[10] M. Yu, J. Wu, J. Shi, O.C. Farokhzad, Nanotechnology for protein delivery: overview and perspectives, J. Contr. Release 240 (2016) 24–37.
[11] S. Mitragotri, P.A. Burke, R. Langer, Overcoming the challenges in administering biopharmaceuticals: formulation and delivery strategies, Nat. Rev. Drug Discov. 13 (2014) 655–672.
[12] Y. Yan, L. Zhou, Z. Sun, D. Song, Y. Cheng, Targeted and intracellular delivery of protein therapeutics by a boronated polymer for the treatment of bone tumors, Bioact. Mater. 7 (2022) 333–340.
[13] H.Y. Kim, J.A. Kang, J.H. Ryou, G.H. Lee, D.S. Choi, D.E. Lee, H.S. Kim, Intracellular protein delivery system using a target-specific repebody and translocation domain of bacterial exotoxin, ACS Chem. Biol. 12 (2017) 2891–2897.
[14] A.M. Asrorov, Z. Gu, K.A. Min, M.C. Shin, Y. Huang, Advances on tumor-targeting delivery of cytotoxic proteins, ACS Pharmacol. Transl. Sci. 3 (2020) 107–118.
[15] A. Yau, J. Lee, Y. Chen, Nanomaterials for protein delivery in anticancer applications, Pharmaceutics 13 (2021) 155.
[16] Y.W. Lee, D.C. Luther, J.A. Kretzmann, A. Burden, T. Jeon, S. Zhai, V.M. Rotello, Protein delivery into the cell cytosol using non-viral nanocarriers, Theranostics 9 (2019) 3280–3292.
[17] S. Guillard, R.R. Minter, R.H. Jackson, Engineering therapeutic proteins for cell entry: the natural approach, Trends Biotechnol. 33 (2015) 163–171.
[18] W. He, J. Yan, F. Sui, S. Wang, X. Su, Y. Qu, Q. Yang, H. Guo, M. Ji, W. Lu, Y. Shao, P. Hou, Turning a Luffa protein into a self-assembled biodegradable nanoplatform for multitargeted cancer therapy, ACS Nano 12 (2018) 11664–11677.
[19] J. Yan, Y. Yao, S. Yan, R. Gao, W. Lu, W. He, Chiral protein supraparticles for tumor suppression and synergistic immunotherapy: an enabling strategy for bioactive supramolecular chirality construction, Nano Lett. 20 (2020) 5844–5852.
[20] T. Daubenfeld, M. Hossann, W.E. Trommer, G. Niedner-Schatteburg, On the contentious sequence and glycosylation motif of the ribosome inactivating plant protein gelonin, Biochem. Biophys. Res. Commun. 333 (2005) 984–989.
[21] M. Hossann, Z. Li, Y. Shi, U. Kreilinger, J. Büttner, P.D. Vogel, J. Yuan, J.G. Wise, W.E. Trommer, Novel immunotoxin: a fusion protein consisting of gelonin and an acetylcholine receptor fragment as a potential immunotherapeutic agent for the treatment of Myasthenia gravis, Protein Expr. Purif. 46 (2006) 73–84.
[22] J. Woodhams, P.J. Lou, P.K. Selbo, A. Mosse, D. Oukrif, A. MacRobert, M. Novelli, Q. Peng, K. Berg, S.G. Bown, Intracellular re-localisation by photochemical internalisation enhances the cytotoxic effect of gelonin — quantitative studies in normal rat liver, J. Contr. Release 142 (2010) 347–353.
[23] F. Stirpe, S. Olsnes, A. Pihl, Gelonin, a new inhibitor of protein synthesis, nontoxic to intact cell, J. Biol. Chem. 255 (1980) 6947–6953.
[24] Z. Li, Y. Qu, H. Li, J. Yuan, Truncations of gelonin lead to a reduction in its cytotoxicity, Toxicology 231 (2007) 129–136.
[25] M. Puri, I. Kaur, M.A. Perugini, R.C. Gupta, Ribosome-inactivating proteins: current status and biomedical applications, Drug Discov. Today 17 (2012) 774–783.
[26] G.B. Ding, G. Wu, B. Li, P. Yang, Z. Li, High-yield expression in Escherichia coli, biophysical characterization, and biological evaluation of plant toxin gelonin, 3 Biotech 9 (2019) 19.
[27] M.C. Shin, J. Zhao, J. Zhang, Y. Huang, H. He, M. Wang, K.A. Min, V.C. Yang, Recombinant TAT–gelonin fusion toxin: synthesis and characterization of heparin/protamine-regulated cell transduction, J. Biomed. Mater. Res. 103 (2015) 409–419.

[28] M.C. Shin, J. Zhang, K.A. Min, K. Lee, C. Moon, J.P. Balthasar, V.C. Yang, Combination of antibody targeting and PTD-mediated intracellular toxin delivery for colorectal cancer therapy, J. Contr. Release 194 (2014) 197–210.
[29] M.C. Shin, J. Zhang, K.A. Min, H. He, A.E. David, Y. Huang, V.C. Yang, PTD-modified attempts for enhanced toxin-based cancer therapy: an in vivo proof-of-concept study, Pharm. Res. (N. Y.) 32 (2015) 2690–2703.
[30] M.C. Shin, K.A. Min, H. Cheong, C. Moon, Y. Huang, H. He, V.C. Yang, Preparation and characterization of gelonin-melittin fusion biotoxin for synergistically enhanced anti-tumor activity, Pharm. Res. (N. Y.) 33 (2016) 2218–2228.
[31] M.C. Shin, J. Zhang, A.E. David, W.E. Trommer, Y.M. Kwon, K.A. Min, J.H. Kim, V. C. Yang, Chemically and biologically synthesized CPP-modified gelonin for enhanced anti-tumor activity, J. Contr. Release 172 (2013) 169–178.
[32] S.H. Ham, K.A. Min, M.C. Shin, Molecular tumor targeting of gelonin by fusion with F3 peptide, Acta Pharmacol. Sin. 38 (2017) 897–906.
[33] M.C. Shina, K.A. Min, H. Cheong, C. Moon, Y. Huang, H. He, V.C. Yang, Tandem-multimeric F3-gelonin fusion toxins for enhanced anti-cancer activity for prostate cancer treatment, Int. J. Pharm. 524 (2017) 101–110.
[34] S. Ham, K.A. Min, J.W. Yang, M.C. Shin, Fusion of gelonin and anti-insulin-like growth factor-1 receptor (IGF-1R) affibody for enhanced brain cancer therapy, Arch Pharm. Res. (Seoul) 40 (2017) 1094–1104.
[35] T. Park, K.A. Min, H. Cheong, C. Moon, M.C. Shin, Genetic engineering and characterization of chlorotoxin-fused gelonin for enhanced glioblastoma therapy, J. Drug Target. 27 (2019) 950–958.
[36] G. Cheng, W. Li, L. Ha, X. Han, S. Hao, Y. Wan, Z. Wang, F. Dong, X. Zou, Y. Mao, S. Y. Zheng, Self-assembly of extracellular vesicle-like metal−organic framework nanoparticles for protection and intracellular delivery of biofunctional proteins, J. Am. Chem. Soc. 140 (2018) 7282–7291.
[37] M.F. Attia, N. Anton, J. Wallyn, Z. Omran, T.F. Vandamme, An overview of active and passive targeting strategies to improve the nanocarriers efficiency to tumour sites, J. Pharm. Pharmacol. 71 (2019) 1185–1198.
[38] W. Gu, F. Meng, R. Haag, Z. Zhong, Actively targeted nanomedicines for precision cancer therapy: concept, construction, challenges and clinical translation, J. Contr. Release 329 (2021) 676–695.
[39] Z. Zhao, H. Meng, N. Wang, M.J. Donovan, T. Fu, M. You, Z. Chen, X. Zhang, W. Tan, A controlled-release nanocarrier with extracellular pH value driven tumor targeting and translocation for drug delivery, Angew. Chem. Int. Ed. 52 (2013) 7487–7491.
[40] G.B. Ding, Y. Wang, Y. Guo, L. Xu, Integrin $\alpha_V\beta_3$-targeted magnetic nanohybrids with enhanced antitumor efficacy, cell cycle arrest ability, and encouraging anti-cell-migration activity, ACS Appl. Mater. Interfaces 6 (2014) 16643–16652.
[41] P. Vaupel, G. Multhoff, Revisiting the Warburg effect: historical dogma versus current understanding, J. Physiol. 599 (2021) 1745–1757.
[42] D. Thévenin, M. An, D.M. Engelman, pHLIP-mediated translocation of membrane-impermeable molecules into cells, Chem. Biol. 16 (2009) 754–762.
[43] M. Kanamala, W.R. Wilson, M. Yang, B.D. Palmer, Z. Wu, Mechanisms and biomaterials in pH-responsive tumour targeted drug delivery: a review, Biomaterials 85 (2016) 152–167.
[44] Y. Zhang, X. Han, G. Nie, Responsive and activable nanomedicines for remodeling the tumor microenvironment, Nat. Protoc. 16 (2021) 405–430.
[45] J.C. Deacon, D.M. Engelman, F.N. Barrera, Targeting acidity in diseased tissues: mechanism and applications of the membrane-inserting peptide, pHLIP, Arch. Biochem. Biophys. 565 (2015) 40–48.
[46] Y.K. Reshetnyak, A. Moshnikova, O.A. Andreev, D.M. Engelman, Targeting acidic diseased tissues by pH-triggered membrane-associated peptide folding, Front. Bioeng. Biotechnol. 8 (2020) 335.
[47] A.M. Demin, A.G. Pershina, A.S. Minin, O.Y. Brikunova, A.M. Murzakaev, N. A. Perekucha, A.V. Romashchenko, O.B. Shevelev, M.A. Uimin, I.V. Byzov, D. Malkeyeva, E. Kiseleva, L.V. Efimova, S.V. Vtorushin, L.M. Ogorodova, V. P. Krasnov, Smart design of a pH-responsive system based on pHLIP-modified magnetite nanoparticles for tumor MRI, ACS Appl. Mater. Interfaces 13 (2021) 36800–36815.
[48] G.B. Ding, X. Ma, X. Meng, P. Yang, R.H. Stauber, Z. Li, pH low insertion peptide (pHLIP)-decorated polymeric nanovehicle for efficient and pH-responsive siRNA translocation, Mater. Des. 212 (2021) 110197.
[49] L.C. Wyatt, J.S. Lewis, O.A. Andreev, Y.K. Reshetnyak, D.M. Engelman, Applications of pHLIP technology for cancer imaging and therapy, Trends Biotechnol. 35 (2017) 653–664.
[50] C.J. Cheng, R. Bahal, I.A. Babar, Z. Pincus, F. Barrera, C. Liu, A. Svoronos, D. T. Braddock, P.M. Glazer, D.M. Engelman, W.M. Saltzman, F.J. Slack, MicroRNA silencing for cancer therapy targeted to the tumour microenvironment, Nature 518 (2015) 107–110.
[51] G.B. Ding, J. Sun, G. Wu, B. Li, P. Yang, Z. Li, G. Nie, Robust anticancer efficacy of a biologically synthesized tumor acidity-responsive and autophagy-inducing functional Beclin 1, ACS Appl. Mater. Interfaces 10 (2018) 5227–5239.
[52] L. Zhai, C. Luo, H. Gao, S. Du, J. Shi, F. Wang, A dual pH-responsive DOX-encapsulated liposome combined with glucose administration enhanced therapeutic efficacy of chemotherapy for cancer, Int. J. Nanomed. 16 (2021) 3185–3199.
[53] H. Han, Y. Hou, X. Chen, P. Zhang, M. Kang, Q. Jin, J. Ji, M. Gao, Metformin-induced stromal depletion to enhance the penetration of gemcitabine-loaded magnetic nanoparticles for pancreatic cancer targeted therapy, J. Am. Chem. Soc. 142 (2020) 4944–4954.
[54] Y. Tian, Y. Zhang, Z. Teng, W. Tian, S. Luo, X. Kong, X. Su, Y. Tang, S. Wang, G. Lu, pH-dependent transmembrane activity of peptide-functionalized gold nanostars for computed tomography/photoacoustic imaging and photothermal therapy, ACS Appl. Mater. Interfaces 9 (2017) 2114–2122.
[55] E.R. Lavallie, Z. Lu, E.A. Diblasio-Smith, L.A. Collins-Racie, J.M. McCoy, Thioredoxin as a fusion partner for production of soluble recombinant proteins in Escherichia coli, Methods Enzymol. 326 (2000) 322–340.
[56] Y. Li, Carrier proteins for fusion expression of antimicrobial peptides in Escherichia coli, Biotechnol. Appl. Biochem. 54 (2009) 1–9.
[57] J.C. Bischof, X. He, Thermal stability of proteins, Ann. N. Y. Acad. Sci. 1066 (2005) 12–33.
[58] R.J. Mrsny, Strategies for targeting protein therapeutics to selected tissues and cells, Expet Opin. Biol. Ther. 4 (2004) 65–73.
[59] M. Ray, Y.W. Lee, F. Scaletti, R. Yu, V.M. Rotello, Intracellular delivery of proteins by nanocarriers, Nanomedicine 12 (2017) 941–952.
[60] E. Brighenti, D. Treré, M. Derenzini, Targeted cancer therapy with ribosome biogenesis inhibitors: a real possibility? Oncotarget 6 (2015) 38617–38627.
[61] Y. Cao, J.D. Marks, J.W. Marks, L.H. Cheung, S. Kim, M.G. Rosenblum, Construction and characterization of novel, recombinant immunotoxins targeting the Her2/neu oncogene product: in vitro and in vivo studies, Cancer Res. 69 (2009) 8987–8995.
[62] Y. Cao, J.W. Marks, Z. Liu, L.H. Cheung, W.N. Hittelman, M.G. Rosenblum, Design optimization and characterization of Her2/neu-targeted immunotoxins: comparative in vitro and in vivo efficacy studies, Oncogene 33 (2014) 429–439.
[63] X. Zhou, J. Qiu, Z. Wang, N. Huang, X. Li, Q. Li, Y. Zhang, C. Zhao, C. Luo, N. Zhang, X. Teng, Z. Chen, X. Liu, X. Yu, W. Wu, Y.Q. Wei, J. Li, In vitro and in vivo anti-tumor activities of anti-EGFR single-chain variable fragment fused with recombinant gelonin toxin, J. Cancer Res. Clin. Oncol. 138 (2012) 1081–1090.